Hydrogen storage in a layered flexible $[Ni_2(btc)(en)_2]_n$ coordination polymer

V. A. Blagojević,[a,b,*] V. Lukić,[c] N. N. Begović,[d] A. M. Maričić[c] and D. M. Minić[e,†]

[a]Institute of Technical Sciences of the Serbian Academy of Sciences and Arts, Belgrade, Serbia.
[b]Vida Fresh Air Corp, Woodbridge, ON, Canada
[c]Technical Faculty Čačak, University of Kragujevac, Serbia.
[d]Institute for General and Physical Chemistry, Belgrade, Serbia.
[e]Faculty of Physical Chemistry, University of Belgrade, Serbia.

Abstract

$[Ni_2(btc)(en)_2]_n$ coordination polymer exhibits a layered two-dimensional structure with weak interaction between the layers. Correlation of experimental measurements and DFT calculations and molecular simulations demonstrated that its structural features, primarily the inherent flexibility of the layered polymeric structure, lead to improved hydrogen storage performance at room temperature, due to significant enhancement in isosteric heats of hydrogen adsorption. Volumetric measurements of hydrogen adsorption at room temperature show up to 0.3 wt.% hydrogen absorbed at 303K and 2.63 bar of hydrogen pressure, with isosteric heats of adsorption of about 12.5 kJ mol^{-1}. Predicted performance at room temperature is 1.8 wt.% at 48 bar and 3.5 wt.% at 100 bar, better than both MOF-5 and NU-100, with calculated values of isosteric heats for adsorption of hydrogen are in 8-13 kJ mol^{-1} range at both 77K and 303K. Grand canonical Monte Carlo calculations show that this material, at 77K, exhibits gravimetric hydrogen densities of more than 10 wt.% (up to 8.3 wt.% excess) with the corresponding volumetric density of at least 66 gL^{-1}, which is comparable to MOF-5, but achieved with considerably smaller surface area of about 2500 m^2g^{-1}. This study shows that layered two-dimensional MOFs could be a step towards MOF systems with significantly higher isosteric heats of adsorption, which could provide better room temperature hydrogen storage capabilities.

* email: vladab64@gmail.com

† email: dminic@ffh.bg.ac.rs

Introduction

Due to high cost and technical requirements, conventional storage of large amounts of hydrogen in its molecular form has proven to be difficult [1, 2]. In recent times, a lot of effort has been expended on development of new materials to store hydrogen with sufficient efficiency to allow use in both stationary and mobile applications [3, 4]. The U. S. Department of Energy has set performance goals for 2015 for on-board automobile storage systems to have densities of 60 mg H_2/g (6 wt.%, gravimetric) and 45 g H_2/L (volumetric), with ultimate goals of 80 mg H_2/g (8 wt.%) and 75 g H_2/L [5, 6]. Given these system goals, a material for practical application would need to have higher capacity when the weight of the tank and associated cooling or regeneration system is considered, and the size and weight of these components will vary substantially depending on whether the material operates by a chemisorption or physisorption mechanism. In the latter case, one of the indicators for promising hydrogen storage materials is the value of physisorption enthalpy for hydrogen: ideally, it should be in 15-25 kJ mol^{-1} range [7-9]. A wide variety of materials has been investigated for their hydrogen storage properties: different carbon materials and carbon-metal nanocomposites [10-15], covalent organic frameworks [16, 17] and porous organic polymers [18, 19]. However, none of them has been able to achieve the performance required for on-board vehicle application, typically providing 5-6 wt.% excess hydrogen capacity at 77K and 20-50 bar. Coordination polymers or metal-organic frameworks (MOFs) have been identified as promising adsorbents for gas and H_2 storage where viable volumetric densities can still be achieved in highly porous structures [20-25]. In this sense, benzene polycarboxylates are a very common group of organic ligands used for synthesis of different MOFs, due to their ability to build high dimensional coordination polymers [26-29].

Ab-initio studies of hydrogen binding to metal-organic frameworks have reported a variety of values for hydrogen binding energies, most of them in 4-12 kJ mol^{-1} range [30-33]. Grand canonical Monte Carlo (GCMC) simulations have been used to predict, with some accuracy, the hydrogen storage capacity of various MOFs at pressures of up to 100 bar [34], and it has been shown that molecular simulation could be a suitable method for high-throughput computational screening of MOFs [35-38]. The combination of quantum chemical calculations and molecular simulations offers the most complete information about hydrogen adsorption in a MOF material, giving the best chance of predicting hydrogen adsorption and storage properties of these materials [39-43].

It has been accepted that hydrogen storage capacity of MOFs is chiefly governed by two factors: structure (adsorbent surface area and free volume) and hydrogen binding energy [7-9, 44]. In most MOFs their high surface area is offset by relatively small values of hydrogen binding energy. So far, most of the effort has been directed at creating materials with very high surface areas, like NU-100 and MOF-210, with surface areas of 6150 and 6230 $m^2\ g^{-1}$ and total hydrogen capacities of 16.4 wt.% at 77K (9.9 wt.% excess) and 70 bar and 17.6 wt.% at 77K and 80 bar, respectively, while large scale screening of MOFs has revealed a number of promising candidates with potential hydrogen storage capacities in 14-20 wt.% range [45]. However, as with all of 3-dimensional rigid MOFs, these can be expected to require low, or even cryogenic, temperatures to achieve high hydrogen uptake, mainly due to relatively low hydrogen binding energies. MOFs typically exhibit hydrogen storage capacities of less than 2 wt.% at room temperature and high pressure (50-100 bar) [46, 47]. Two-dimensional MOF systems have typically exhibited inferior hydrogen storage properties due to relatively low surface area of 200-1600 $m^2\ g^{-1}$ [48-50], where hydrogen is stored in the pores of the two-dimensional structure, while the inter-layer space remains inaccessible.

Herein we report hydrogen adsorption performance of flexible coordination polymer $[Ni_2(btc)(en)_2]_n$ [51] at room temperature and normal pressure complemented with molecular simulation of hydrogen adsorption. It is shown that its structural features: two-dimensional layers with weak inter-layer interactions, provide tremendous adaptability to the introduction of hydrogen into the lattice and allow hydrogen adsorption performance comparable and, in some aspects, superior to that of 3-dimensional MOFs with significantly higher surface area. This structure provides access to the inter-layer space, unlike typical two-dimensional MOFs, allowing it to achieve higher available surface for adsorption. Its room temperature performance is 0.3 wt.% at 2.6 bar with isosteric heat of adsorption of 12-13 kJ mol^{-1}, and predicted to be about 1.8 wt.% at 48 bar and 3.5 wt.% at 100 bar with

isosteric heat of around 8.5 kJ mol^{-1}. While its low pressure performance is inferior to some other room temperature hydrogen storage materials (0.3-0.7 wt.% at 1 atm and 298K) [10-12], its high pressure predicted performance is superior or comparable to even the best of the available systems, like graphene foam decorated with Pt nanoparticles (3.19 wt.% at 100 bar) [52]. Its predicted high pressure performance at room temperature is also superior to well known MOFs like MOF-5 and NU-100 (1.65 wt.% at 48 bar and 1.19 wt.% at 90 bar, respectively).

Experimental

Materials and Methods

$[Ni_2(btc)(en)_2]_n$ coordination polymer was synthesized by dehydration of $[Ni_2(en)_2(H_2O)_6(btc)]\cdot 4H_2O$ (btc = tetraion of benzene tetracarboxylic acid; en = ethylene diamine). $[Ni_2(en)_2(H_2O)_6(btc)]\cdot 4H_2O$ was synthesized according to the procedure used in Ref. 53, 54. The resulting blue powder was then dried at 175°C for 30 min. Dehydration causes a change in colour from light blue to light green [51]. X-ray powder diffraction (XRD) patterns were obtained using Philips PW−1710 automated diffractometer, using Cu Kα line, operated at 40 kV and 30 mA, in Bragg-Brentano geometry. The instrument was equipped with diffracted beam curved graphite monochromator and Xe filled proportional counter. Diffraction data were collected in 2θ ranges of 4 – 35°(counting for 5s for routine identification) and 8 – 80º, (counting for 12.5s for Rietveld refinement), at 0.02° steps. Fixed 1° divergence and 0.1 mm receiving slits were used and silicon powder was used as a standard for calibration of the diffractometer. XRD measurements were performed on a sample that was additionally dried at 60°C under reduced pressure of 0.05 bar for 30 min to remove any residual water.

TG measurements of gravimetric argon adsorption were conducted on TA SDT 2960 instrument using 99.999% argon gas additionally purified using molecular sieves. Cycle 1 represents the measurement of the sample dried at 60°C under reduced pressure of 0.05 bar for 30 min, while Cycle 2 represents the repeated subsequent measurement of the sample loaded with argon during Cycle 1, without removal from the instrument and argon atmosphere. Heating rate was constant at 5 K min^{-1} on heating and 2 K min^{-1} on cooling. Volumetric hydrogen storage capacity measurements were conducted in a sealed chamber with a volume of 120.53 ml. Sample with a mass of 0.3341 mg was dried and placed in the chamber, which was then purged with hydrogen and sealed. The sample was then kept at 1.01 bar (1atm) of hydrogen pressure for 18 hours. Measurements at different pressures (1.01–2.63 bar; 1–2.6 atm) were performed on the same sample, consecutively by gradually increasing the hydrogen pressure in the chamber, without removing the sample or decreasing pressure. Each measurement was performed at a constant volume, by heating the chamber from 30 to 180°C at a constant heating rate of 6°C min^{-1}, and then cooling the chamber to 30°C at a rate of 2°C. Changes in pressure during both heating and cooling were recorded at 5°C intervals. Hydrogen storage capacity at each pressure was calculated from desorption curve, using the difference in observed pressure in the chamber at 180°C with and without the sample (baseline). The pressure difference was recalculated to mass using the Van der Waals equation of state.

Computational Details

Since Ni in $[Ni_2(btc)(en)_2]_n$ coordination polymer can exhibit two types of coordination: octahedral and square-planar, each of which would result in a somewhat different layered structure, DFT calculations were performed on model systems of $[Ni_2(btc)(en)_2]_n$ coordination polymer representing each of these structures to determine the average binding energy per hydrogen molecule, as well as whether the changes in coordination sphere of Ni would have a significant effect on hydrogen adsorption of $[Ni_2(btc)(en)_2]_n$ coordination polymer. The calculations were performed using Gaussian [55] and ORCA software packages [56]. Gaussian package was used for structure optimization and frequency analysis, using the hybrid HF/DFT method using a combination of the three-parameter Becke [57] exchange functional with the Lee-Yang-Parr (B3LYP) [58] non-local correlation functional. Orca calculations used the hybrid HF/DFT method with a combination of the three-parameter Becke exchange functional combined with Perdew's [59] (BP86) non-local correlation functional. The basis set used was split valence with polarization functions (SV(P)), except for Ni atoms and the adsorbed hydrogen molecules, where triple-zeta valence basis set with polarization functions (TZVP) was applied [60]. Each model system consists of four interconnected Ni(btc)(en) units, creating a single layer, with the second Ni(en) group omitted from each unit.

Molecular simulations were performed using GULP v4.3 [61, 62] and Grand Canonical Monte Carlo

(GCMC) calculations were performed using Music [63] software packages, both utilizing Universal Force Field [64]. Supercells of $[Ni_2(btc)(en)_2]_n$ with dimensions of 4x4x4 were used for the calculations at 77K and 8x8x8 for the calculations at 303K. For calculations with MOF-5, supercells with dimensions of 2x2x2 and 4x4x4 were used, which provided similar system volume to the supercells of $[Ni_2(btc)(en)_2]_n$. GCMC calculations were performed on a rigid cell with $5 \cdot 10^6$ iterations and 0.4 probability for insertion and deletion and 0.1 probability for rotation and translation of a hydrogen molecule, respectively.

Results and discussion

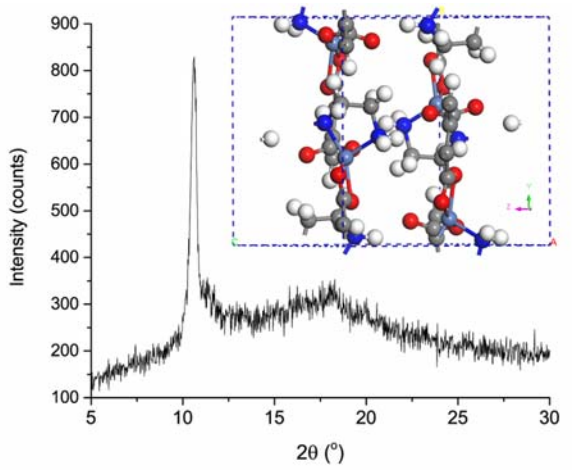

Figure 1. XRD diffraction pattern of $[Ni_2(pyr)(en)_2]_n$ coordination polymer, with structure shown as inset.

Figure 1 shows XRD pattern of $[Ni_2(btc)(en)_2]_n$ coordination polymer sample that was prepared from $[Ni_2(en)_2(H_2O)_6(btc)]\cdot 4H_2O$ complex by thermal treatment in flowing nitrogen gas at 450K for 30 min. Its structure can be best described as two-dimensional laminar structure with weak hydrogen-bond connectivity between the individual layers. The basic two-dimensional framework consists of Ni atoms with chelately coordinated 1,2,4,5–benzenetetracarboxylic acid (BTCA) anions, where each Ni atom is connected to two BTCA molecules, while each BTCA is connected to four Ni atoms. Ethylene diamine is coordinated to Ni in a plane roughly perpendicular to the plane of the basic framework, providing hydrogen bonding in the third dimension and completing the octahedral coordination sphere around Ni. Calculated density of the coordination polymer is 1.7 gcm^{-3}. BET measurement of Ni coordination polymer indicates negligible accessible surface area (1.6-2 $m^2\ g^{-1}$) for nitrogen adsorption at 77K (Figure S1, Supplement) and zero effective porosity.

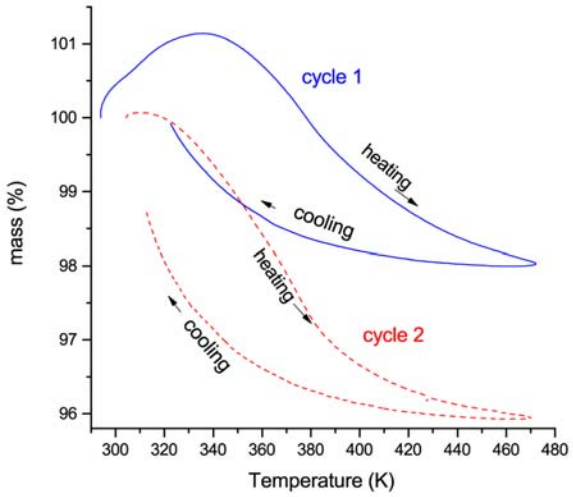

Figure 2. Argon adsorption in TG for $[Ni_2(pyr)(en)_2]_n$ coordination polymer sample during two heating cycles.

Gas adsorption of the coordination polymer was tested using TG measurements of adsorption of argon (Figure 2). Coordination polymer exhibits relatively high reversible adsorption of argon gas in 300-470 K temperature region of around 4 wt. %, corresponding to around 26 cm^3g^{-1} or 0.5 molecules of argon adsorbed per monomer unit of the coordination polymer. By simply taking into account the molar mass difference between Ar and H_2 (about 20:1), it could be expected that the coordination polymer sample exhibits around 0.2 wt.% hydrogen adsorption at 1.01 bar (1atm) and room temperature. This suggests that the lattice at room temperature likely exhibits larger volume compared to the lattice at 77K, allowing argon to enter and be absorbed in the interior of the crystal grains. Volumetric hydrogen desorption measurements (Figure 3) of the sample loaded under 1.01 bar (1atm) of hydrogen pressure shows that, in a dynamic experiment, on heating to 454 K, the sample releases about 0.1 wt.% hydrogen. Hydrogen desorption measurement at 2.63 bar (2.6atm) pressure shows that the sample releases about 0.3 wt.% of hydrogen on heating to 453K. On cooling, the sample takes the hydrogen back in, showing that desorption of 0.3 wt.% of hydrogen is fully reversible.

Table 1. Hydrogen capacity on desorption at 303K and different initial hydrogen pressures

Pressure (bar)	Hydrogen Capacity (wt. %)
1.01	0.103
1.82	0.234
2.23	0.268
2.63	0.297

Table 1 shows hydrogen capacity at different pressures calculated from adsorption/desorption experiments shown in the Supplement. Significantly lower hydrogen capacity at 1.01 bar (1atm) and the shape of the adsorption curve on cooling indicate that the sample was not fully loaded before hydrogen desorption measurement. Assuming linear dependence of hydrogen capacity, expected in this region of temperature and pressure, and using the other three points, approximate capacity at 1.01 bar (1atm) would be 0.17 wt.%, and the rate of increase of capacity with pressure 0.079 wt.% per bar. Using Clausius-Clapeyron equation, isosteric heats of hydrogen adsorption and desorption were calculated for different initial pressures (Supplement). The average values were: 13±2 $kJmol^{-1}$ for desorption and 12±2 $kJmol^{-1}$ for adsorption, measured on heating and cooling cycles, respectively. This is on the high end of isosteric heats achieved in MOF materials and about double the typical room temperature isosteric heats observed in most well known MOFs [8, 9].

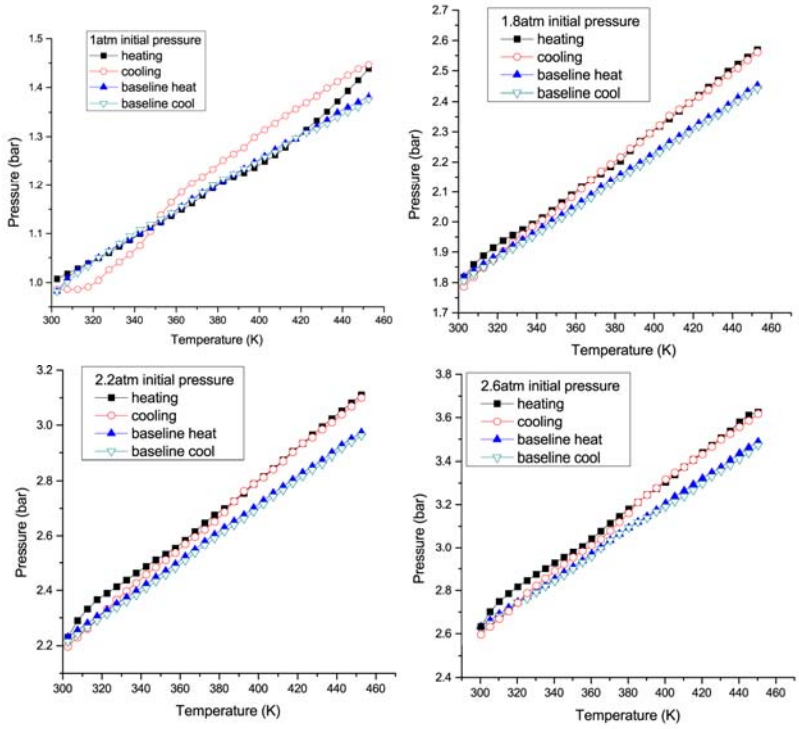

Figure 3. Hydrogen adsorption and desorption during cooling/heating of $[Ni_2(pyr)(en)_2]_n$ coordination polymer at different initial hydrogen pressures.

When the coordination polymer sample was heated to 388K at 2.63 bar (2.6 atm) initial hydrogen pressure, and then equilibrated at that temperature for 30 min at a constant hydrogen pressure of around 3.14 bar (3.1 atm), it showed increased hydrogen uptake on cooling (Figure 4) of around 0.09 wt.%. Since hydrogen pressure in the chamber showed no anomalous behavior during the experiment (that would indicate a leak), this suggests that the observed hydrogen uptake comes from the expansion of the crystal lattice of the coordination polymer. This is also in line with the detected crystal lattice contraction at 77K during BET measurement, which showed no appreciable free surface area or volume, highlighting the flexible nature of the coordination polymer's layered structure. Multiple experiments have been performed on the same sample, which was then analyzed again, and it can be reported that there was no observable loss in crystallinity or hydrogen storage performance after 30 cycles.

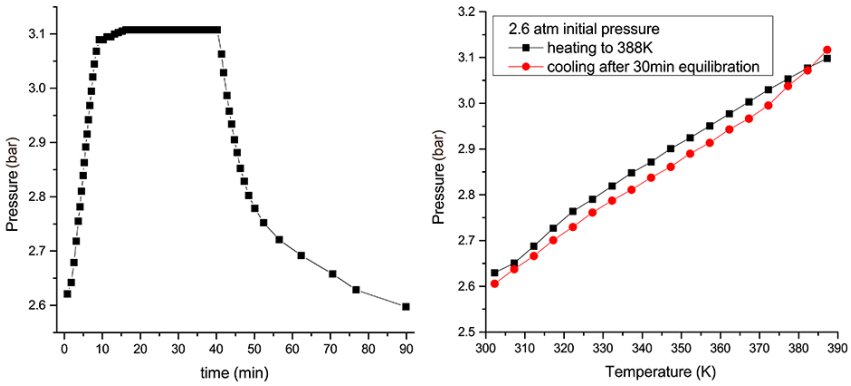

Figure 4. Hydrogen desorption and subsequent adsorption after equilibration at 388K for 30min

DFT Calculations

In order to investigate hydrogen adsorption properties of $[Ni_2(btc)(en)_2]_n$ in more detail, DFT calculations were used to determine the binding energy of hydrogen molecules to the structure of the coordination polymer. Since Ni atom exhibits two possible spin states: quintuplet and singlet, both of these were examined regarding hydrogen binding (Figure 5), with the more stable quintuplet system [51] exhibits much more favorable hydrogen binding properties. A truncated tetramer model system was constructed to investigate its hydrogen binding properties in more detail, and hydrogen molecules were sequentially added to one surface of the system, which was then optimized (Supplement). A combination of BP86 and MP2 calculations using ORCA software package show an average binding energy of around 9 $kJmol^{-1}$ (Table S1 in Supplement), for interaction with a single layer, corresponding to a double hydrogen layer in the real system. B3LYP calculations performed using Gaussian 09 software yielded slightly higher values: an average binding energy of 12.1 kJ mol^{-1}, corresponding to a hydrogen capacity of about 4.5 wt.%. The values of binding energies in these calculations correspond to the physical system where each layer of the coordination polymer is saturated with hydrogen molecules, i.e. there is a double hydrogen layer between two neighboring coordination polymer layers. At lower hydrogen content, it is possible to have a single layer of hydrogen molecules interacting simultaneously with both neighboring coordination polymer layers, with potentially higher values of binding energy.

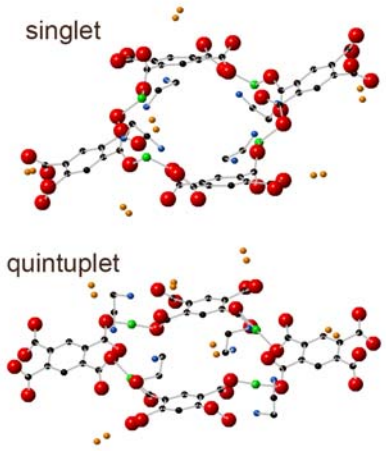

Figure 5. Optimized model tetramer structures in different electronic states, with six adsorbed hydrogen molecules (structural hydrogen atoms are omitted for clarity)

Molecular simulations

In order to investigate in more depth the effect of the flexible structure of the coordination polymer on hydrogen adsorption properties, molecular simulation was used to simulate lattice expansion on hydrogen uptake and the dependence of hydrogen adsorption on lattice expansion. Therefore, simulated annealing and geometry optimization was used to obtain structures with different relative lattice volumes, while GCMC calculations were used to calculate hydrogen adsorption isotherms and adsorption energy distributions at both 77 and 303K for each of these individual structures (Figure 6).

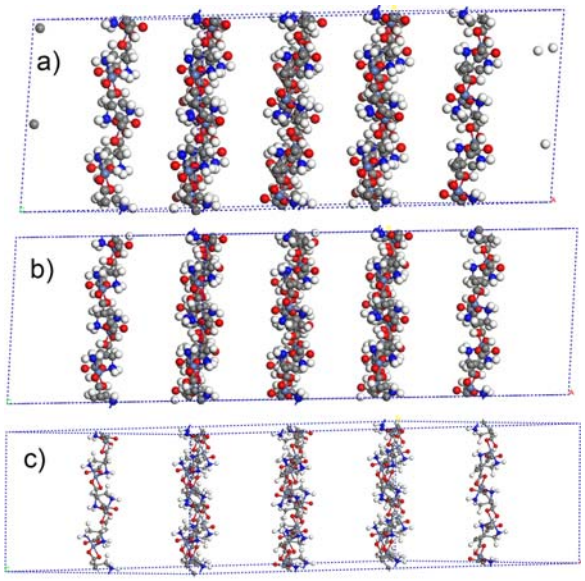

Figure 6. A perspective view of three polymer lattices with different relative lattice volumes (a: 160%; b: 195%; c: 235%)

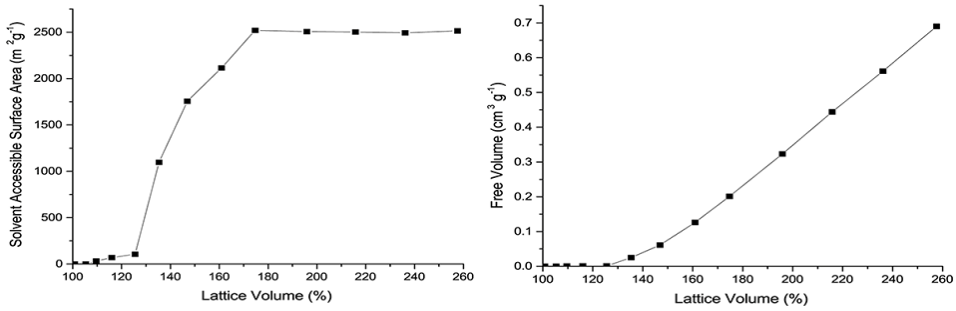

Figure 7. Change in solvent accessible surface area and free volume for hydrogen on lattice expansion (the volume of the experimentally obtained structure is taken as 100%).

gas adsorption. Figure 7 shows that both SA and FV for hydrogen increase rapidly after lattice expands by around 30%. SA reaches a plateau at relative lattice volume of around 175%, and an inter-planar distance of around 9 Å, the point where the structure is able to accommodate a double hydrogen layer, with a value of around 2500 m^2 g^{-1}. Naturally, further lattice expansion only contributes to the increase of FV.

H_2 adsorption at 77K

Figure 8. shows adsorption energy distributions for structures with different lattice expansion and hydrogen content and the corresponding average adsorption energy. For lattice expansion of 125% and hydrogen content of 2.5 wt.%, the average adsorption energy is around 11 $kJmol^{-1}$, which is consistent with the results of DFT calculations. However, this indicates that the strength of the interaction of

Molecular simulations show that the structure of the coordination polymer in a-b plane is quite rigid, with minimal changes in bond lengths and angles (Supplement). However, since there are no covalent of coordination bonds along c-axis, the coordination polymer is able to adapt completely to hydrogen addition to the system by expanding along this axis. The consequence is that the two-dimensional polymer layers gradually separate depending on the amount of hydrogen in the system, which leads to an increase in solvent accessible surface area (SA) and free volume (FV). The experimental crystal structure from XRD measurements, which was obtained after drying under reduced pressure, exhibits both zero surface area and zero free volume, just like the coordination polymer at 77K in BET measurement. However, lattice expansion due to introduction of gas molecules into the lattice increases both SA and FV, allowing

hydrogen with the MOF matrix is underestimated by the molecular simulation, because DFT calculations correspond to significantly higher hydrogen content and double hydrogen layer configuration. This can also be correlated with the previously observed underestimation of hydrogen adsorption at 303K. The average adsorption energy then drops to about 9.4 at 4.3 wt.% of hydrogen and 8.4 at 5.9 wt.%, after which the decline slows down considerably (MOF-5 exhibits adsorption energies around 8 $kJmol^{-1}$ in the calculation at 77K). This occurs because, at lower hydrogen content, hydrogen molecules can interact with two polymer layers, while at higher hydrogen content, double hydrogen layer is gradually formed, where each hydrogen molecule can interact only with one polymer layer, resulting in lower adsorption energy. After the formation of the full double layer, at around 6 wt.% of hydrogen, further addition of hydrogen only creates local reorganization and

disruption of the double layer, leading to relatively slow decline in the value of the average adsorption energy with addition of hydrogen into the lattice.

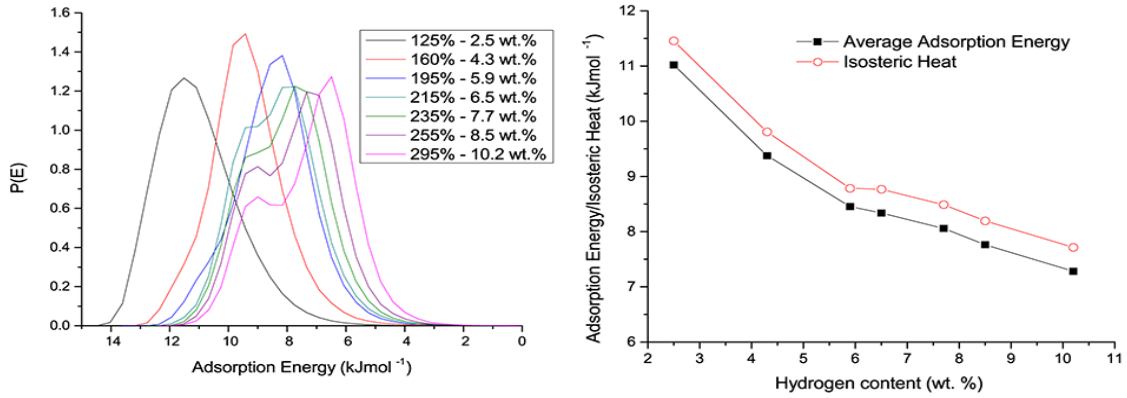

Figure 8. Adsorption energy distribution from GCMC calculations for hydrogen adsorption (left); Dependence of the average adsorption energy and isosteric heat on hydrogen content (right)

Figure 9. shows calculated adsorption isotherms at 77K for selected structures with different lattice volume, while Figure 10. shows excess hydrogen capacity for selected structures. This shows how hydrogen capacity changes dramatically with increase in relative lattice volume: from 2.5 wt.% at 125% to 10.2 wt.% at 295% relative lattice volume. Additional calculations compared the performance of $[Ni_2(btc)(en)_2]_n$ system at 295% relative lattice volume to MOF-5 calculated with similar system size (Supplement). These showed similar performance at 77K, and since MOF-5 exhibits a surface area of more than 4000 m^2g^{-1} [65], compared to about 2500 m^2g^{-1} for $[Ni_2(btc)(en)_2]_n$, this indicates considerably stronger hydrogen sorption in $[Ni_2(btc)(en)_2]_n$.

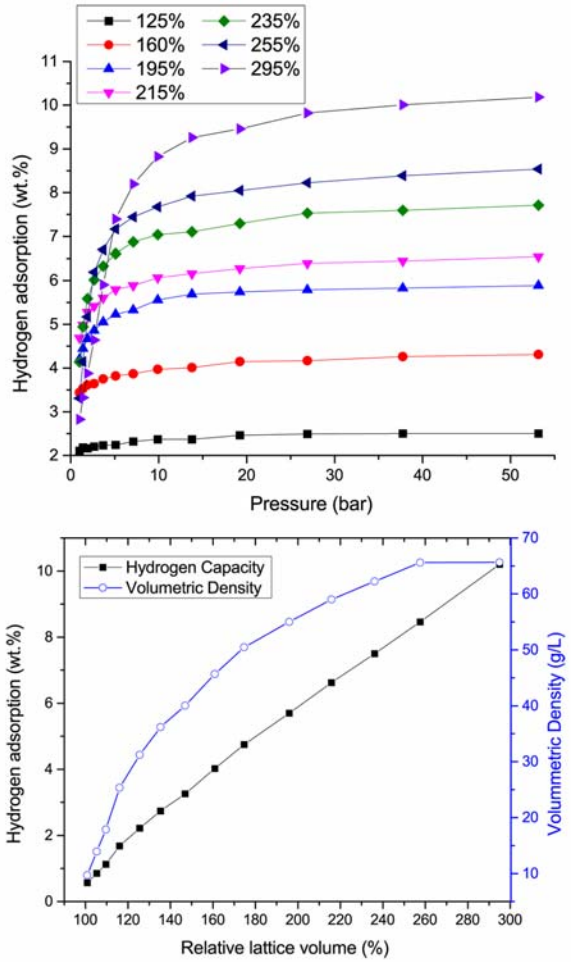

Figure 9. Hydrogen adsorption isotherms from GCMC calculations (top); Calculated gravimetric and volumetric hydrogen density at 77 K and 50 bar for structures with different relative lattice volumes (bottom).

H_2 adsorption at 303 K

Figure 11. shows simulated isotherms for hydrogen adsorption at 303K and 1-50 bar pressure, for systems with different relative lattice volumes. The calculations significantly underestimate performance of the experimental system, shown in Table 1, of 0.2-0.3 wt.% in 1-3 bar region of hydrogen pressures. At

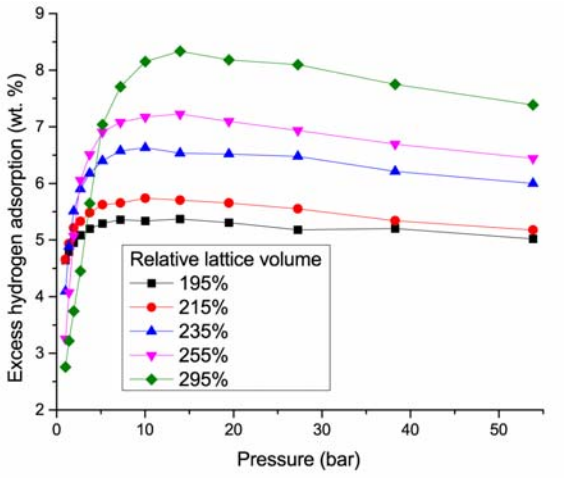

Figure 10. Calculated excess hydrogen capacity at 77K for structures with different lattice volumes.

the highest relative lattice volume of 295%, the slope of the line is 0.012 wt.% per bar, while the experimental system exhibits 0.079 wt.% per bar. The isotherms for argon adsorption at 303K and 0.1-1 bar pressure show the impact of the flexibility of the structure on adsorption (Figure 8). Argon adsorption increases with lattice expansion and reaches a maximum at around 150% relative lattice volume, after which, argon adsorption decreases.

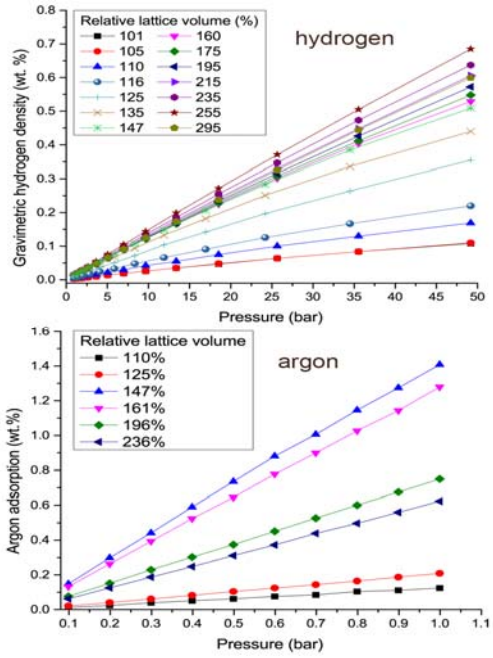

Figure 11. GCMC simulation isotherms for hydrogen (top) and argon (bottom) adsorption at 303K for systems with different relative crystal lattice volume

This is due to creation of an optimal single layer of argon gas in the interlayer space of the coordination polymer, where each argon atom interacts with two layers.Further lattice expansion disrupts argon interaction with one of the layers, leading to a significant decrease in binding energy and a corresponding decrease in argon adsorption (Supplement). This shows that this coordination polymer would adapt to the amount of adsorbed gas through lattice expansion to achieve optimal level of interaction with the gas. However, it is worth noting that the maximum simulated argon adsorption is 1.4 wt.%, compared to a reversible adsorption of around 4 wt.% obtained gravimetrically in the experiment. This means that molecular simulations significantly underestimate argon adsorption in the coordination polymer system around room temperature.

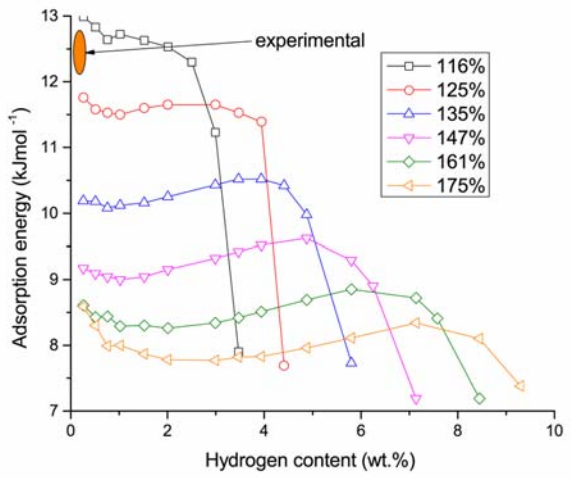

Figure 12. Adsorption energy as a dependence on hydrogen content, calculated from NVT molecular simulations at 303K, for structures with different relative lattice volumes.

Figure 12. shows the results of NVT molecular simulations at 303K for different hydrogen contents, in systems with different relative lattice volumes. These show that the adsorption enthalpy decreases from around 13 to around 8.5 kJ mol^{-1} with increase in relative lattice volume from 116 to 175%, while maximum hydrogen content (estimated from the point of sharp decrease in adsorption enthalpy) increases from around 2 to around 7 wt.%. At 175% lattice expansion, the system achieved maximum surface area. The corresponding isosteric heats for hydrogen adsorption (from GCMC calculations) are in 8−12 kJ mol^{-1} range. In comparison, MOF-5 system exhibits isosteric heats of around 5 kJ mol^{-1} [45]. This demonstrates the main advantage of a layered two-dimensional coordination polymer over the rigid three-dimensional structure: flexibility of the layered structure results in significantly higher isosteric heats for hydrogen adsorption at room temperature, allowing the system to find the optimal balance of heat of adsorption and surface area.

Since all of the simulated systems and, generally, other MOF systems in the literature, exhibit linear increase in hydrogen adsorption with pressure in 1-50 bar region [44-47], depending mainly on the value of the isosteric heat of adsorption and surface area. Using the equation of Firlej et al. [7], we can estimate the performance of $[Ni_2(btc)(en)_2]_n$ coordination polymer to be around 3.5 wt.% at 100 bar and 298K (with surface area of 2520 m^2g^{-1} and isosteric heat of adsorption of 8.5 kJ mol^{-1}). This compares favorably to 0.5 wt.% at 10 bar and 1.65 wt.% at 48 bar for MOF-5 or 1.19 wt.% at 90 bar for SNU-77H [44, 45]. Using the volumetric density data in Figure 9. as a guide, we could estimate that the corresponding volumetric density would probably be 25 gL^{-1}. This suggests that this type of coordination polymer could exhibit superior hydrogen storage properties at temperatures near the room temperature, where its flexible structure could enhance its performance and remedy one of the main flaws of rigid MOFs: low heat of adsorption.

Conclusions

$[Ni_2(btc)(en)_2]_n$ coordination polymer exhibits relatively good hydrogen adsorption capability of 0.3 wt.% at room temperature and pressure of 2.63 bar (2.6 atm). Its structure compares favorably to typical two-dimensional MOFs [48-50], because it provides access to the inter-layer space, significantly increasing the available surface area for adsorption. In addition, flexible structure that expands on adsorption and contracts on desorption would reduce the amount of unused hydrogen during charge/discharge cycle. Using molecular simulation and experimental results at low pressures of 1.01-2.63 bar (1-2.6 atm) and room temperature for a projection of behavior at high pressures, suggests that the projected hydrogen storage capacity at room temperature and 100 bar is around 3.5 wt.% and 25 gL^{-1}. Its projected performance at room temperature is significantly better than that of MOF-5 and NU-100 (1.65 wt.% at 48 bar and 1.19 wt.% at 90 bar, respectively) [44, 45] and comparable to graphene foam decorated with Pt nanoparticles (3.19 wt.% at 100 bar) [52]. This can be attributed to significantly higher values of isosteric heats (8−12 kJ mol^{-1} compared to 5-6 kJ mol^{-1} in MOF-5 and NU-100), due to the flexibility of the system, which provides stronger lattice-hydrogen interactions. The calculated total hydrogen capacity of around 10.2 wt.% at 77K and 53 bar, and maximum calculated excess hydrogen capacity of around 8.3 wt.% at 77K and 14 bar, compare well to the excess hydrogen adsorption of NU-100 of around 9.9 wt.% [45], even though $[Ni_2(btc)(en)_2]_n$ exhibits considerably lower surface area (around 2500 compared to >6100 m^2g^{-1}). Molecular simulations and DFT calculations suggest that the isosteric heats for hydrogen adsorption are in region of 8-13 kJ mol^{-1} for a wide range of hydrogen content (up to around 8 wt.%) at 77K, comparable or superior to most MOFs. The main focus of development of MOF materials in the past decade has been an increase in available surface area for adsorption, with relatively little progress being made in increasing the isosteric heats for hydrogen adsorption. This study of $[Ni_2(btc)(en)_2]_n$ shows that a

new approach, using flexible layered 2-dimensional instead of rigid 3-dimensional structures, could provide a step towards producing systems with significantly higher isosteric heats of adsorption, while achieving relatively high surface area. This would be a significant step forward in achieving MOF materials capable of significant room temperature hydrogen storage capacities.

Acknowledgements

This work was supported by the Ministry of Education, Science and Technological Development of the Republic of Serbia under the project OI 172057.

References

[1] Ogden JM. Prospects for building a hydrogen energy infrastructure. Annu. Rev. Energy Environ. 1999;24:227-279.

[2] Ritter JA, Ebner AD, Wang J, Zidan R. Implementing a hydrogen economy. Mater. Today 2003;6:18-23.

[3] Schlapbach L, Züttel A. Hydrogen-storage materials for mobile applications. Nature 2001;414:353-8.

[4] Durbin DJ, Malardier–Jugroot C. Review of hydrogen storage techniques for on board vehicle applications. Int. J. Hydrogen Energy 2013;38:14595-14617.

[5] Hydrogen, Fuel Cells, & Infrastructure Technologies Program: Multiyear Research, Development, and Demonstration Plan; U.S. Department of Energy, February 2005, Chapter 3, http://www.eere.energy.gov/hydrogenandfuelcells/mypp/

[6] Basic Research Needs for the Hydrogen Economy, report of the Basic Energy Sciences Workshop on Hydrogen Production, Storage, and Use, U.S. Department of Energy, May 13–15, 2005, http://www.sc.doe.gov/bes/

[7] Firlej L, Pfeifer P, Kuchta B. Understanding Universal Adsorption Limits for Hydrogen Storage in Nano Porous Systems. Adv. Mater. 2013;25:5971-5974.

[8] Bae YS, Snurr RQ. Optimal isosteric heat of adsorption for hydrogen storage and delivery using metal–organic frameworks, Micropor. Mesopor. Mat. 2010;132:300-303.

[9] Ahluwalia RK, Peng J-K, Hua TQ. Sorbent material property requirements for on-board hydrogen storage for automotive fuel cell systems. Int. J. Hydrogen Energy 2015;40:6373-6390.

[10] Bao D, Gao P, Shen X, Chang Ch, Wang L, Wang Y, Chen Y, Zhou X, Sun S, Li G, Yang P. Mechanical ball-milling preparation of fullerene/cobalt core/shell nanocomposites with high electrochemical hydrogen storage ability. ACS Appl. Mater. Inter. 2014;6:2902-2909

[11] Sano N, Taniguchi K, Tamon H. Hydrogen storage in porous single-walled carbon nanohorns dispersed with Pd-Ni alloy nanoparticles. J. Phys. Chem. C 2014;118:3402-3408.

[12] Ensafi AA, Jafari-Asl M, Nabiyan A, Rezaei B, Dinari M, Hydrogen storage in hybrid of layered double hydroxides/reduced graphene oxide using spillover mechanism, Energy 2016;99:103-114.

[13] Baburin IA, Klechnikov A, Mercier G, Talyzin A, Seifert G. Hydrogen adsorption by perforated graphene. Int. J. Hydrogen Energy 2015;40:6594-6599.

[14] Benard P, Chahine R. Determination of the adsorption isotherms of hydrogen on activated carbons above the critical temperature of the adsorbate over wide temperature and pressure ranges. Langmuir 2001:1950-5.

[15] Kabbour H, Baumann TF, Satcher JH, Saulnier A, Ahn CC. Towards new candidates for hydrogen storage: high surface area carbon aerogels. Chem. Mater. 2006;18(26):6085-7.

[16] Han SS, Furukawa H, Yaghi OM, Goddard WA. Covalent organic frameworks as exceptional hydrogen storage materials. J. Am. Chem. Soc. 2008;138:11580-1.

[17] Furukawa H, Yaghi OM. Storage of hydrogen, methane, and carbon dioxide in highly porous covalent organic frameworks for clean energy applications. J. Am. Chem. Soc. 2009;131:8875-83.

[18] Liu DJ, Yuan S, White D, Mason A, Reprogle B. Hydrogen storage through porous organic polymers (POPs). FY 2010 annual progress report, DOE hydrogen and fuel cells program. 2011. p. 495-8.

[19] Yuan S, White D, Mason A, Liu DJ. Porous organic polymers containing carborane for hydrogen storage. Int. J. Energy. Res. 2013;37:732-40.

[20] Wong–Foy AG, Matzger AJ, Yaghi OM. Exceptional H_2 Saturation Uptake in Microporous Metal−Organic Frameworks. J. Am. Chem. Soc. 2006;128:3494-3495

[21] Kumar P, Kim K-H, Kwon EE, Szulejko JE, Metal–organic frameworks for the control and management of air quality: advances and future direction. J. Mater. Chem. A 2016;4:345-361.

[22] Li H, Eddaoudi M, O'Keeffe M, Yaghi OM. Design and synthesis of an exceptionally stable and highly porous metal-organic framework. Nature 1999;202:276-279.

[23] Furukawa H, Ko N, Go YB, Aratani N, Choi SB, Choi E, Yazaydin AO, Snurr RQ, O'Keeffe M., Kim J, Yaghi OM. Ultrahigh Porosity in Metal-Organic Frameworks. Science 2010;329:424-428.

[24] Saga D, Zacharia R, Lafi L, Cossement D, Chahine R. Synthesis, characterization and hydrogen adsorption properties of metal–organic framework Al-TCBPB. Int. J. Hydrogen Energy 2012;37:5100-5107.

[25] Wu X, Wang R, Yang H, Wang W, Cai W, Li Q. Ultrahigh hydrogen storage capacity of novel porous aromatic frameworks. J. Mater. Chem. A 2015;3:10724-10729.

[26] Kim JC, Jo H, Lough AJ, Cho J, Lee U, Pyun SY. Polymeric nickel(II) and copper(II) complexes with btc^{2-} ions as bridging ligands (btc^{2-}=1,2,4,5-benzenetetracarboxylic acid dianion). Inorg. Chem. Comm. 2003;6:474-477.

[27] Fabelo O, Pasan J, Lloret F, Julve M, Ruiz-Perez C. Structural versatility in cobalt(II) complexes with 1,2,4,5-benzenetetracarboxylic acid (H_4bta) and 4,4′-bipyridine-N,N′-dioxide (dpo). CrystEngComm 2007;9:815-827.

[28] Fabelo O, Pasan J, Canadillas-Delgado L., Delgado FS, Labrador A, Lloret F, Julve M, Ruiz-Perez C. (4, 4) Rectangular Lattices of Cobalt (II) with 1, 2, 4, 5-Benzenetetracarboxylic Acid: Influence of the Packing in the Crystal Structure. Crys. Growth Des. 2008;8:3984-3992.

[29] Zhang LP, Ma JF, Yang J, Pang YY, Ma JC. Series of 2D and 3D Coordination Polymers Based on 1,2,3,4-Benzenetetracarboxylate and N-Donor Ligands: Synthesis, Topological Structures, and Photoluminescent Properties. Inorg. Chem. 2010;49:1535-1550.

[30] Panella B, Hirscher M, Pütter H, Müller U. Hydrogen Adsorption in Metal–Organic Frameworks: Cu-MOFs and Zn-MOFs Compared. Adv. Funct. Mater. 2006;16:520-524.

[31] Jeloaica L, Sidis V. DFT investigation of the adsorption of atomic hydrogen on a cluster-model graphite surface. Chem. Phys. Lett. 1999;300:157-162.

[32] Wu H, Zhou W, Yildirim T. Hydrogen Storage in a Prototypical Zeolitic Imidazolate Framework-8. J. Am. Chem. Soc. 2007;129:5314-5315.

[33] Yeganegi S, Sokhanvaran V. Ab initio study of hydrogen adsorption on Zn2(NDC)2(diPyTz) metal-organic framework decorated with alkali and alkaline earth metal cations. Int. J. Hydrogen Energy 2014;39:14008-14017.

[34] Frost H, Duren T, Snurr RQ, Effects of Surface Area, Free Volume, and Heat of Adsorption on Hydrogen Uptake in Metal−Organic Frameworks. J. Phys. Chem. B 2006;110:9565-9570.

[35] Farha OK, Yazaydin AO, Eryazici I, Malliakis CD, Hauser BG, Kanatzidis MG, Nguyen ST, Snurr RQ, Hupp JT. De novo synthesis of a metal–organic framework material featuring ultrahigh surface area and gas storage capacities. Nature Chem. 2010;2:944-948

[36] Wilmer CE, Leaf M, Lee CY, Farha OK, Hauser BG, Hupp JT, Snurr RQ. Large-scale screening of hypothetical metal–organic frameworks. Nature Chem. 2012;4:83-89

[37] Goldsmith J, Wong-Foy AG, Cafarella MJ, Siegel DJ. Theoretical Limits of Hydrogen Storage in Metal–Organic Frameworks: Opportunities and Trade-Offs. Chem. Mater. 2013;25:3373-3382.

[38] Gomez DA, Toda J, Sastre G. Screening of hypothetical metal–organic frameworks for H_2 storage. Phys. Chem. Chem. Phys. 2014;16:19001-19010.

[39] Basdogan Y, Keskin S. Simulation and modelling of MOFs for hydrogen storage. CrystEngComm 2015;17:261-275.

[40] Volkova EI, Vakhrushev AV, Suyetin M. Improved design of metal-organic frameworks for efficient hydrogen storage at ambient temperature: A multiscale theoretical investigation. Int. J. Hydrogen Energy 2014;39:8347-8350.

[41] Luzan SM, Jung H, Chun H, Talyzin AV, Hydrogen storage in Co-and Zn-based metal-organic frameworks at ambient temperature. Int. J. Hydrogen Energy 2009;34:9754-59.

[42] Wang Y, Fang M, Li Y, Liang J, Shi W, Chen J, Cheng P. A porous 3d-4f heterometallic metal–organic framework for hydrogen storage. Int. J. Hydrogen Energy 2010;35:8166-8170.

[43] Prasanth KP, Rallapalli P, Raj MC, Bajaj HC, Jasra RV. Enhanced hydrogen sorption in single walled carbon nanotube incorporated MIL-101 composite metal–organic framework. Int. J. Hydrogen Energy 2011;36:7594-7601.

[44] Langmi HW, Ren J, North B, Mathe M, Bessarbov D. Hydrogen Storage in Metal-Organic Frameworks: A Review. Electrochim. Acta, 2014;128:368-392.

[45] Colon YJ, Snurr RQ. High-throughput computational screening of metal–organic frameworks. Chem. Soc. Rev. 2014;43:5735-5749.

[46] Zacharia R, Cossement D, Lafi L, Chahine R, Volumetric hydrogen sorption capacity of monoliths prepared by mechanical densification of MOF-177. J. Mater. Chem. 2010;20:2145-2151.

[47] Saha D, Wei Z, Deng S. Equilibrium, kinetics and enthalpy of hydrogen adsorption in MOF-177. Int. J. Hydrogen Energy 2008;33:7479-7488;

[48] Park KS, Ni Z, Cote AP, Choi JY, Huang R, Urbe-Romo FJ, et al. Exceptional chemical and thermal stability of zeolitic imidazolate frameworks. PNAS 2006;103(27):10186-91.

[49] Dinca M, Yu AF, Long JR. Microporous metal-organic frameworks incorporating 1,4-benzeneditetrazolate: syntheses, structures, and hydrogen storage properties. J Am Chem Soc 2006;128:8904-13.

[50] Ozturk Z, Kose DA, Sahin ZS, Ozkan G, Asan A. Novel 2D micro-porous Metal-Organic Framework for hydrogen storage. Int. J. Hydrogen Energy 2016;41:12167-12174.

[51] Begović NN, Blagojević VA, Ostojić SB, Radulović AM, Poleti D, Minić DM, Thermally activated 3D to 2D structural transformation of $[Ni_2(en)_2(H_2O)_6(pyr)]\cdot 4H_2O$ flexible coordination polymer. Mater. Chem. Phys. 2015;149-150:105-112.

[52] Jung H, Park KT, Gueye MN, So SH, Park CR. Bio-inspired graphene foam decorated with Pt nanoparticles for hydrogen storage at room temperature. Int. J. Hydrogen Energy 2016;41:5019-5027.

[53] Poleti D, Stojakovic DR, Preselnik BV, Herak RM. Structure of binuclear hexa-aqua-μ-[1,2,4,5-benzene-tetra-carboxylato(4–)]-bis-(ethylenedi-amine)dinickel(II) tetrahydrate. Acta Cryst. 1988;C44:242-245.

[54] Zdravković JD, Poleti D, Rogan J, Begović NN, Blagojević VA, Vasić MM, Minić DM. Thermal stability and degradation of binuclear hexaaqua-bis(ethylenediamine)-(μ 2-pyromellitato)dinickel(II) tetrahydrate. J. Therm. Anal. Calorim. 2016;123:1715-1726.

[55] Frisch MJ, Trucks GW, Pople JA. Gaussian 09, revision B.2. Gaussian Inc., Pittsburgh, PA, 2009.

[56] Neese F. The ORCA program system. Wiley Interdiscip. Rev.: Comput. Mol. Sci. 2012;2:73-78.

[57] Becke AD. Density-functional exchange-energy approximation with correct asymptotic behavior. Phys. Rev. A 1988;38:3098.

[58] Lee C, Yang W, Parr RG. Development of the Colle-Salvetti correlation-energy formula into a functional of the electron density. Phys. Rev. B 1988;37:785.

[59] Perdew JP. Density-functional approximation for the correlation energy of the inhomogeneous electron gas. Phys. Rev. B 1986;33:8822.

[60] Ahlrichs R. Many body perturbation calculations and coupled electron pair models. Comp. Phys. Comm. 1979;17:31-45.

[61] Gale JD. Empirical potential derivation for ionic materials. Philosophical Magazine B 1996;73:3-19.

[62] Gale JD. Analytical Free Energy Minimization of Silica Polymorphs. J. Phys. Chem. B 1998;102:5423-5431.

[63] Gupta A, Chempath S, Sanborn MJ, Clark LA, Snurr RQ. Object-oriented programming paradigms for molecular modeling. Mol. Simul. 2003;29:29-46.

[64] Rappe AK, Casewit CJ, Colwell KS, Goddard WA III, Skiff WM. UFF, a full periodic table force field for molecular mechanics and molecular dynamics simulations. J. Am. Chem. Soc. 1992;114:10024-10035.

[65] Eddaoudi M, Kim J, Rosi N, Vodak D, Wachter J, O'Keeffe M, Yaghi OM. Systematic Design of Pore Size and Functionality in Isoreticular MOFs and Their Application in Methane Storage. Science 2002;295:469-472.